Astronomy & Astrophysics manuscript no. aa1268-04
(DOI: will be inserted by hand later)

A solar active region loop compared with a 2D MHD model

C. Gontikakis[1], G. J. D. Petrie[2,⋆], H. C. Dara[1], and K. Tsinganos[2]

[1] Research Center of Astronomy and Applied Mathematics, Academy of Athens, Soranou Efessiou 4, 115 27, Athens, Greece
e-mail: [cgontik;edara]@cc.uoa.gr
[2] IASA and Section of Astrophysics, Astronomy and Mechanics, Department of Physics, University of Athens, Panepistimiopolis, 157 84, Athens, Greece
e-mail: gpetrie@hao.ucar.edu;tsingan@phys.uoa.gr

Received 10 May 2004 / Accepted 5 January 2005

Abstract. We analyzed a coronal loop observed with the *Normal Incidence Spectrometer* (NIS), which is part of the *Coronal Diagnostic Spectrometer* (CDS) on board the *Solar and Heliospheric Observatory* (SOHO). The measured Doppler shifts and proper motions along the selected loop strongly indicate unidirectional flows. Analysing the Emission Measure Curves of the observed spectral lines, we estimated that the temperature along the loop was about 380 000 K. We adapted a solution of the ideal MHD steady equations to our set of measurements. The derived energy balance along the loop, as well as the advantages/disadvantages of this MHD model for understanding the characteristics of solar coronal loops are discussed.

Key words. Sun: corona – Sun: magnetic fields – magnetohydrodynamics (MHD) – Sun: UV radiation

1. Introduction

Loops are one of the basic features of the solar corona. They are curved, filamentary features, connecting regions with opposite photosperic magnetic fields. They represent a basic component of active regions in the Extreme UltraViolet (EUV) and their understanding should contribute to the solution of the coronal heating problem.

A specific class of loops are the so-called "cool EUV" loops, with temperatures of $T < 10^6$ K (Bray et al. 1991). Their systematic study began with the analysis of *Skylab* data (Foukal 1975, 1976), where it was stated that only the presence of flows could explain the height reached in the corona by these cool structures. The use of *Skylab* observations helped us understand that cool loops are different objects to the "hot" ones ($\geq 10^6$ K), since very often they are nearby but not co-spatial with them (Dere 1982; Habbal et al. 1985). Moreover, Sheeley (1980) noticed a large time variability of the cool loops in contrast to the hot ones.

After the launch of SOHO, a number of studies on active region loops were based on observations from CDS/NIS and from the *Extreme Ultraviolet Imaging Telescope* (EIT) in the EUV. In a study of five active regions, observed with CDS/NIS, Fludra et al. (1997) confirmed the frequent morphological distinctiveness of the cooler loops. Moreover, observations in the O V, 630 Å line, again with CDS/NIS, showed that cool loops present Doppler shifts all along their length of the order of $\pm(50-60)$ km s^{-1} that, in some cases, can reach values of $\simeq 200-300$ km s^{-1} (Brekke 1997; Kjeldseth-Moe & Brekke 1998; Brekke et al. 1997). Furthermore, their time variability can be as short as 3 min, as is deduced by movies obtained by the *Transition Region And Coronal Explorer* (TRACE), although some loops appear stable for up to about 3 h. It is believed that measurements of the temperature along loops will be able to discern their proper heating mechanism. However, temperature measurements carried out along $1.5-2. \times 10^6$ K loops, using the ratio of the narrowband filters 171, 195 Å from TRACE and EIT (Lenz et al. 2004; Aschwanden et al. 1999) seem in contradiction to the measurements carried out with spectral data from CDS/NIS (Schmelz et al. 2001). A lot of effort has been dedicated to the solution of this controversy (e.g. Martens et al. 2002; Aschwanden 2002) to clarify whether the low spatial resolution of CDS or the low spectral resolution of the narrowband instruments is to blame for a bias in the temperature measurements. Recently, Del Zanna & Mason (2003) pointed out that part of the problem lies in the proper correction of the measured loop emission for the diffuse background emission along the line of sight (LOS). They showed that the two emissions seem to originate from plasma in a different thermal state. Furthermore, they noticed that the response function of the 195 Å TRACE narrowband was computed with out of date atomic data parameters, suggesting that the scientific results based on the 171/195 ratio should be revisited.

However, the methods that are used to deduce plasma temperatures from narrowbands or spectral line intensities use as-

⋆ Visiting Fellowship, High Altitude Observatory & Scientific Computing Division, National Center for Atmospheric Research, PO Box 3000, Boulder, CO 80307-3000, USA.

sumptions that are sometimes difficult to justify and could lead to more than one solution, as is discussed by Judge & McIntosh (2000).

Another approach could be to use a model for the computation of plasma parameters, such as the temperature and to compare the computed intensity flux with the observations in order to check whether the model can reproduce the observations (e.g. Aschwanden et al. 2000; Reale & Peres 2000; Del Zanna & Mason 2003; and Petrie et al. 2003).

The first loops succesfully described by a model were the very hot (3×10^6–10^7 K) X-ray ones for which the hydrostatic assumption holds (Rosner et al. 1978). However it seems that the less hot ones (10^6–$2. \times 10^6$ K), observed by EIT and TRACE, are not in hydrostatic equilibrium in general (Aschwanden et al. 2001; Winebarger et al. 2003). The hydrostatic scale height at 10^6–2×10^6 K is smaller than the height usually reached by these loops.

An attempt to model the intensities and flows along cool loops (Peres 1997), observed in the O v 630 Å line by CDS, concluded that steady hydrodynamic siphon flows could not explain the loop apex brightness. The same author, using a time-dependent calculation, suggests that these discrepancies could be a result of the impulsive nature of the heating. The disadvantages of a hydrodynamic unidirectional flow approach to explain TRACE loop observations are described in Patsourakos et al. (2004).

However, Petrie et al. (2003) showed that steady flows can be more successful in reproducing loop measurements if one takes into account self consistently the magnetic forces in the momentum equation. They were able to match the measured electron densities, temperatures and flows along the loops with the results from a steady 2D MHD model. Moreover, it was concluded that flows have an important influence on the loop energy balance. This means that flows, along with temperature and density, are physical quantities that should be carefully determined in order to proceed in constraining the loop heating function. This is in contrast to the common belief that plasma velocities do not affect the heating balance of a coronal loop significantly and therefore static models are adequate to determine the heating function, since coronal plasma kinetic energies make up only a small proportion of the total energy budget.

In the present study we selected an active region loop with time scales of about 1 h and a dominant unidirectional flow for comparison with the MHD model. Note that this is a cool loop, observed in transition region lines, with temperature much lower than the $\simeq 10^6$ K studied in Petrie et al. (2003). The emphasis in this paper is on a detailed presentation of our measurements, since the MHD model was already presented in Petrie et al. (2003). Thus, Sects. 2 and 3 are devoted to the observations and their critical analysis, while in Sect. 4 our results are fitted to the MHD model. The advantages and disadvantages of our modelling technique are briefly and critically discussed in Sect. 5, while our main conclusions are given in Sect. 6.

2. Observations, data reduction and measured flows in O v 630 Å

The NIS spectrometer on CDS simultanously records two spectral bands: the first (NIS 1) covers the 308–381 Å part of the solar spectrum and the second one (NIS 2) the 513–633 Å part. The spectral resolutions are respectively 0.32 Å and 0.54 Å. Usually, only some selected parts of the spectrum (e.g. some spectral lines plus their adjacent continuum) are kept to speed up the tranfer of the data to the ground. Each single exposure records a field of view of a 240″ long, North-South oriented slit. Square fields of $4' \times 4'$ are obtained by activating a scan mirror in the East-West direction. On October 26 and 27, 1999, CDS/NIS observed the active region NOAA 8737 on the S-W limb of the Sun, executing 218 scans with an 11 minute cadence (Fredvik et al. 2002). Each slit exposure simultaneously recorded six spectral lines emitted by the ions He I, O III, O V, Ne VI, Mg IX, and Fe XVI at the wavelengths 584 Å, 599 Å, 630 Å, 562 Å, 368 Å and 361 Å, sampling the solar atmosphere in temperatures of the upper chromosphere, the transition region and the corona. The active region was also observed by SUMER (Fredvik et al. 2002) and Yohkoh, which recorded a flare.

We selected the CDS data taken between 8:40 and 09:23 UT and for their treatment, we corrected the CCD bias, flatfield, burn-in effects and cosmic rays (see Del Zanna 1999, for an introduction to CDS data reduction). From each individual spectral profile of the O v 630 Å line, we subtracted the adjacent pseudo-continuum, formed by the scattered light from the solar disk (see Del-Zanna & Mason 2003). We also corrected the mis-alignement between the two spectral bands of NIS, using the NIS_ROTATE routine.

Then, we applied a fitting routine to these profiles to produce intensity and Doppler shift maps. As the images were taken after the SOHO recovery, we had to take into account the change of the PSF of the spectrometer, which produces broadened line profiles that differ from a purely Gaussian shape (Thompson 1999). The Doppler shift maps were corrected for the geometric distortion. As there is no wavelength calibration on-board, we made the assumption that the Doppler shift is equal to zero at a quiet region very close to the limb, because there the Doppler shift of O v 630 Å has statistically very small values (see in Peter & Judge 1999, their Fig. 4). Figure 1 presents nine consecutive intensiy images, presenting the loop from its birth to its disappearance. Each row of intensity images is followed by the row with the corresponding Dopplergrams. In panels 1 and 2 of the first row, the loop segment AB is filled from the northern footpoint whereas in panel 3, it is full of bright plasma. Moreover, in the Dopplergrams, the north footpoint is redshifted contrary to the south one. These facts could be interpreted as material flow from the north footpoint to the south one and, because of a possible inclination of the loop plane away from the observer, we observe these values of Doppler shifts along its length. The loop is visible from 09:02 to 10:06 UT and disappears in raster 10:06–10:17 UT. The corresponding Dopplergrams show that the velocity pattern along its length is the same during this time.

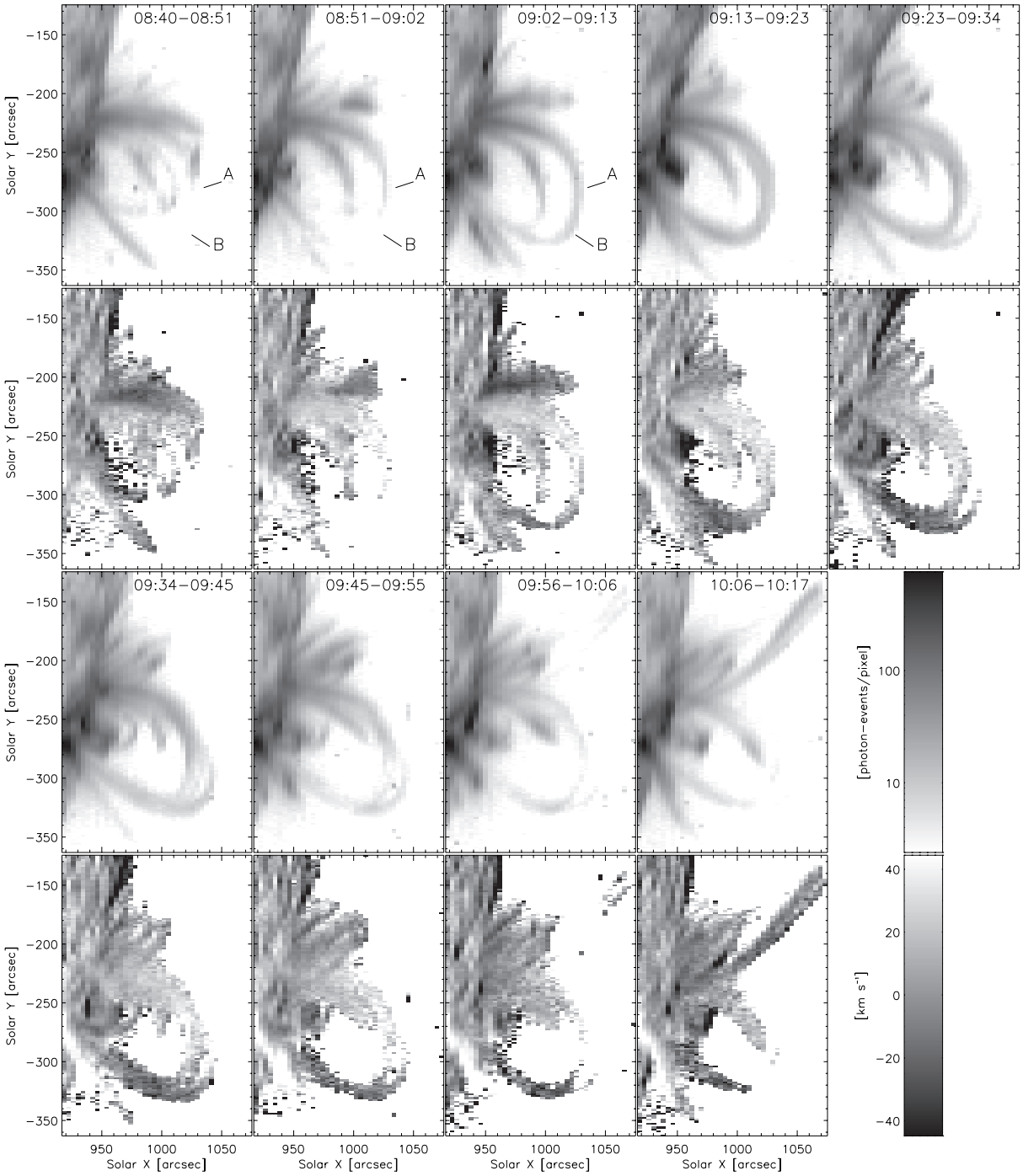

Fig. 1. Total line intensity maps (*first, third rows*) and the corresponding Dopplergrams (*second and fourth rows*) in O v 630 Å (maximum ion concentration at 250 000 K), showing the evolution of the active region. The segments A and B in panels 2 and 3 show the selected loop. The loop evolution in panels 2 and 3 of the first row and the corresponding Dopplergrams indicate that the loop is replenished from its northern footpoint by a unidirectional flow. The first row images indicate proper motions of the order of 30 ± 6 km s^{-1}. The pattern of the loop remains roughly unchanged from 09:02 to 09:55 UT. The loop is fainter in the 09:56−10:06 UT raster and disappears in the 10:06−10:17 UT one. The Dopplergrams show a constant flow pattern along the loop for all its life time. We used a logarithmic scale for the intensities to enhance the loop contrast.

In an effort to study the loop physical parameters, we sampled the loop in the 09:13−09:23 UT raster (see Fig. 2). For each spectral profile selected along the loop, we chose up to 4 more profiles nearby, but outside the loop (Fig. 2, panel 2). We subtracted the mean of these nearby profiles from the loop ones, to correct for the background effect. The background in our case is composed of photons that are emitted along the LOS but outside the loop (the plasma is optically thin). The fitting of the corrected profiles provided the Doppler shift and the total intensity along the loop. These measurements are presented

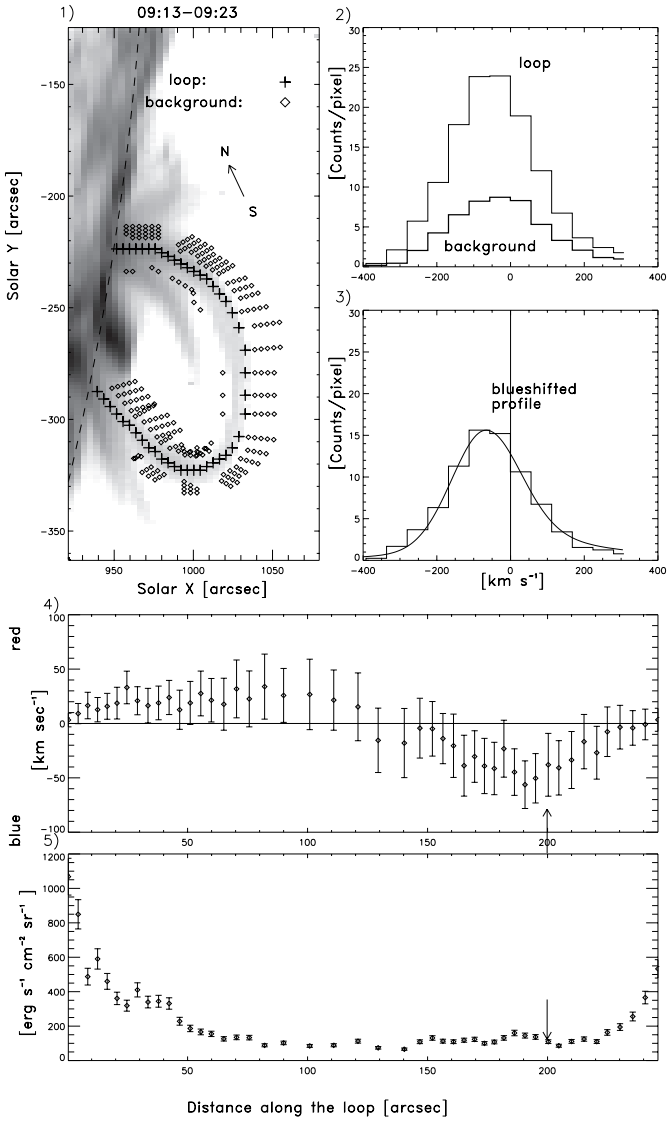

Fig. 2. A thorough study of the loop in O v 630 Å. In panel 1, crosses are the sampling points along the loop and diamonds are the corresponding background ones. Panel 2 shows one spectral profile taken on the loop and the corresponding background one (dispersion axis is in km s^{-1}). Panel 3 is the loop profile of panel 2 after the subtraction of the background profile. The smooth line is computed by the fitting procedure and estimates the total intensity and Doppler shift. Panel 4 shows the Doppler shift along the loop (starting from the northern footpoint). Panel 5 shows the flux emitted from the loop plasma along the loop in physical units. The two arrows in panels 4 and 5 indicate the Doppler shift and intensity values derived from the individual spectral profile of panel 3.

in Fig. 2, panels 4 and 5, along with errorbars, derived by the fitting process. Even with the large error bars, a clear variation of the Doppler shift from red (positive velocities) to blue shift is present.

In panels 4 and 5 of Fig. 2 the total projected length of the loop is 245″. To estimate the maximum length of the loop, we used the MDI magnetogram of 24/10/1999, where the studied active region (NOAA 8737) has a maximum horizontal length of ≃200″. Supposing that the loop is semicircular and, in a rather extreme case, its footpoint separation is of the size of the active region, we estimated that its maximum length is about 314″ which corresponds to 225 Mm. This estimation assumes that the loop connects two opposite polarities from the same active region. This must be the case since NOAA 8737 is isolated and far from other active regions visible on the magnetogram. The loop length will be used for the calculation of the Alfvén travel time in Sect. 4.

3. Emission measure analysis along the loop

3.1. Estimation of the loop temperature

In Fig. 3, the images of the six spectral lines recorded during 6 rasters, from 08:19 to 09:23 UT, are presented. We wanted to select the spectral lines in which the loop has the same morphology and time evolution as in O v 630 Å. We noticed that the loop morphology in the O v 630 Å and Ne vi 563 Å lines is almost identical in the 6 rasters. In the 09:13–09:23 UT raster that we analysed, the Mg ix line image has a loop which is partly cospatial with the O v and Ne vi one but with a less similar morphology (Fig. 4). Furthermore, the time evolution of the Mg ix loop is different from O v, Ne vi ones, as it can be seen in the 6 rasters. On the other hand, we cannot see the loop in O iii and in He i only its footpoints could be guessed. In the hotter Fe xvi 361 Å line, no loop features seem co-spatial with the O v ones.

Therefore, it seems that the considered loop plasma emits mostly in the temperature range of O v 630 Å, Ne vi 562 Å lines, if we take into account the loop morphology and time evolution.

We will include the Mg ix 368 Å spectral line further in the analysis, but not in the estimation of the loop temperature for the reasons mentioned above as well as for those discussed in the following paragraphs.

Similarly to the case of O v, we computed the total intensity for the Ne vi, Mg ix lines along the loop. We derived the contribution functions $G(T)$ for the three spectral lines, with the CHIANTI package (Dere et al. 1997) using a constant electron density of $N_e = 10^9$ cm^{-3}, considering a hybrid abundance for the solar corona (Fludra & Schmelz 1999). Assuming that the plasma is in ionization equilibrium, we applied the Mazzotta et al. (1998) ionization fractions. For each point along the loop and for the three spectral lines (O v, 630 Å, Ne vi 562 Å, Mg ix 368 Å), we computed the ratios $I/G(T)$, where (I) is the total line intensity.

In Fig. 5, panel 1, each of these ratios is presented, for a single point along the loop, as double dashed curves, in order to account for uncertainties that will be discussed in Sect. 3.2. An emission measure distribution of the loop plasma along the LOS, sharply peaked at 380 000 K, at the crossing point of the O v and Ne vi curves, can reproduce the loop brightness in these two spectral lines. A similar sharp distribution that would reproduce the loop brightness in the three lines (O v 630, Ne vi 562, Mg ix 368 Å) should peak at ≃500 000 K, but would need an electron density of 10^{12} cm^{-3}. Such a high density cannot be supported in such a gradually stratified manner as implied by the flux profiles over the timescales observed.

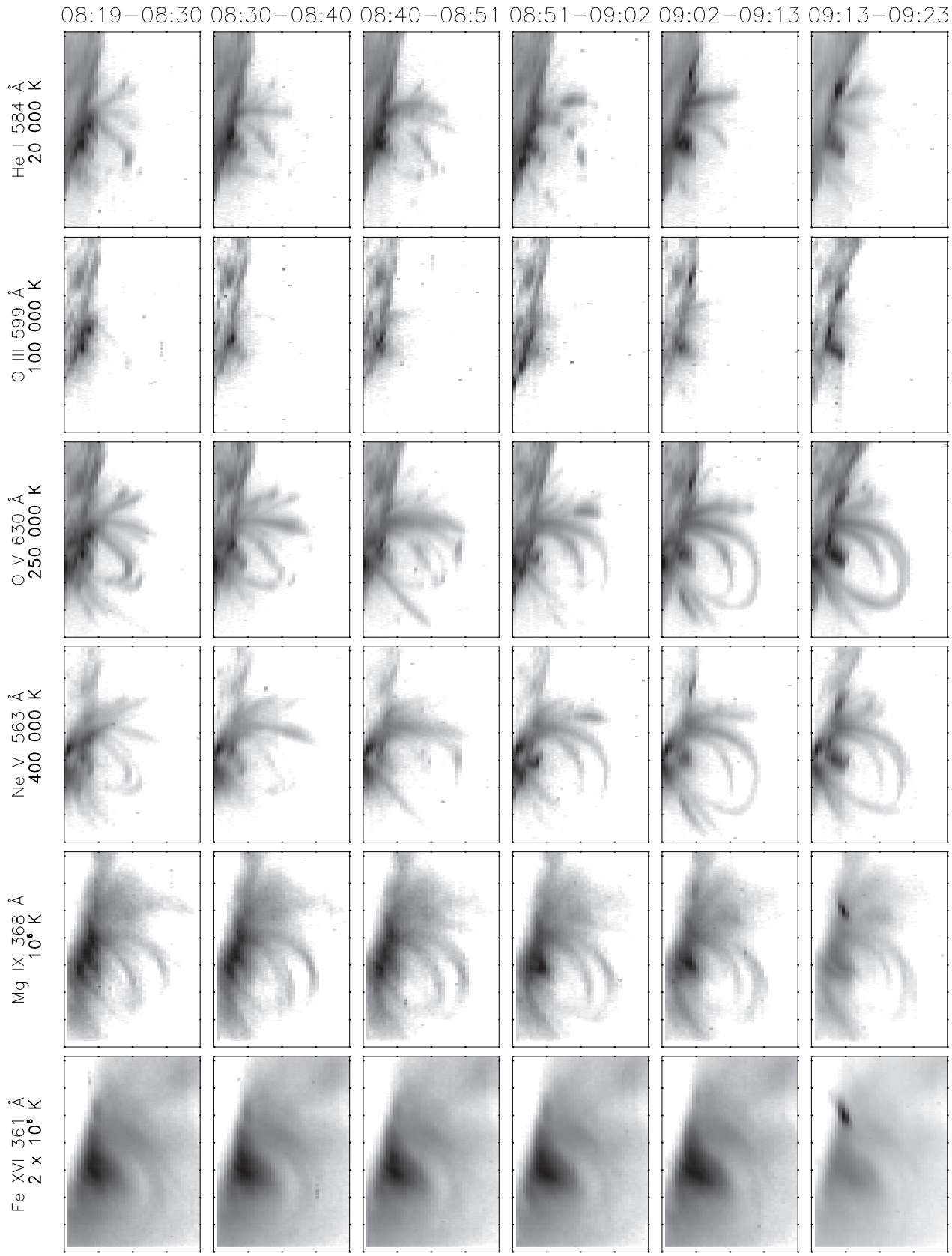

Fig. 3. Images from all spectral lines, observed during 6 rasters, ordered by increasing temperature of maximum ion concentration. The Mg IX and Fe XVI images co-alignment was corrected to account for the spatial offset between NIS-1 (308−379 Å) and NIS-2 (513−633 Å) parts of the CDS detector. The loop seems co-aligned in the O V 630 Å, Ne VI 563 Å and Mg IX 368 Å spectral lines. However, the loop evolution is similar in the O V and Ne VI lines, while this is not the case for the Mg IX line. As in Fig. 1 the unidirectional flow is evident by comparing the individual images in O V and Ne VI.

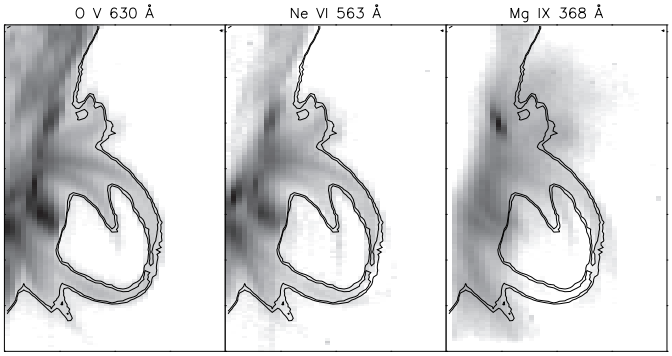

Fig. 4. Intensity images of the O V 630 Å, Ne VI 563 Å and Mg IX 368 Å lines, (09:13−09:23 UT) with the contours of O V 630 Å line superimposed. Whereas the O V contours match well the Ne VI image, they match only part of the Mg IX loop. Furthermore, the Mg IX loop apex seems shifted to the right relative to the O V contours.

Therefore, we considered that the plasma temperature of the loop is defined at the crossing point of the O V and Ne VI curves (Fig. 5). The temperature estimated with this method is almost constant along the loop, of the order of 380 000 K. We did not include the Mg IX measurement in the loop temperature estimation because we think that it originates from a different loop. This choice is supported by the fact that there is a general belief (Fludra et al. 1997) that cool loops (i.d. O V, Ne VI ones) are different to the hot ones (seen in Mg IX lines in this case).

3.2. Uncertainties in the temperature estimation

The computations of the $G(T)$ functions include some assumptions that need to be discussed. For example, ion populations at the upflowing loop footpoint, where plasma probably flows across strong temperature gradients, should shift from the assumed ionization equilibrium values (see Spadaro et al. 1991). The time needed for the underabundant O V, Ne VI ions to reach their equilibrium values can be estimated as the inverse of the ionization rates of O IV, Ne V respectively. We estimated these quantities from the corresponding table of Shull & Van Steenberg (1982), considering a temperature of 380 000 K and an electron density of 10^9 cm^{-3}. The lifetimes we found are 2 s and 17 s respectively. If we suppose a flow speed of about 50 km s^{-1}, at the upflowing footpoint, the equilibrium values of the populations will be reached within the first 1.5″ from the upflowing footpoint of the loop. This value is a very small fraction of the loop length and therefore we can neglect this effect in our estimations. Another case of departure from ionization equilibrium can hold if the loop is subject to time variations of the temperature along its length, due to heating or cooling events (see for example the simulations performed by Bradshaw & Mason 2003a,b). In the case of our loop, it seems that such variations could have occurred during the "birth" of the loop, 20 min before the period that we analysed (see Fig. 1). Following the previous reasoning, we found that the longest timescale, computed from the ionization and recombination rates for the two cooler ions, is the recombination rate of O V, which is roughly equal to 1 min. From the previous simple calculation we think that the ionization equilibrium holds for O V and Ne VI in the measurement we carried out.

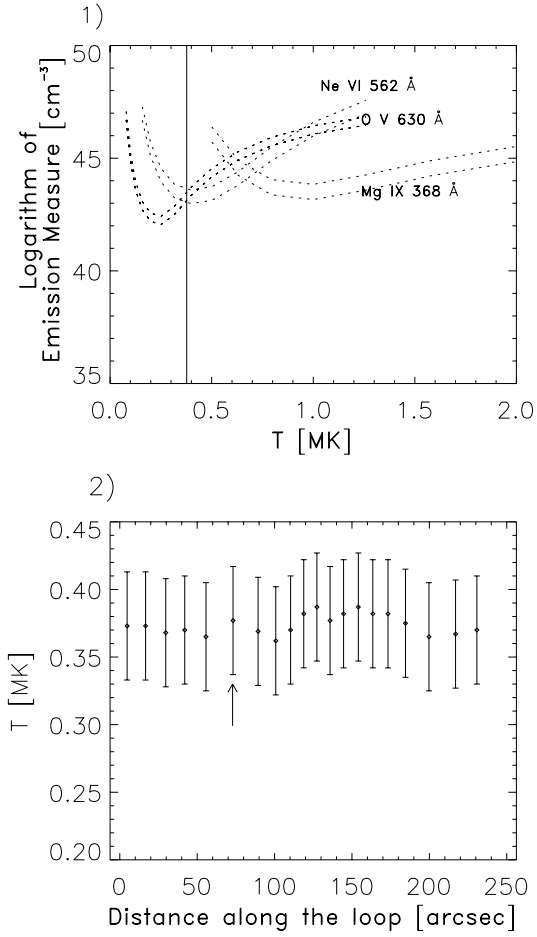

Fig. 5. In panel 1, the emission measures for O V 630 Å, Ne VI 562 Å and Mg IX 368 Å for a given part of the loop are plotted as functions of temperature. The loop plasma temperature is estimated at the crossing point between the O V and Ne VI curves. The dashed lines show the effect of the uncertainties discussed in Sect. 3.1. They produce two extreme crossing points for the emission measure curves and are translated to error bars on the temperature. Panel 2 shows the derived temperature along the loop. The arrow points to the temperature measurement presented in panel 1.

The fact that the available spectral lines originate from different elements brings uncertainties that are due to the element abundances. Schmelz et al. (2001) studied a sample of 33 non-flaring active regions and concluded that the Ne/O ratio present a variation of a factor 4. Moreover, the CDS calibrated intensities have an accuracy of the order of 30% (Del Zanna et al. 2001). Taking into account these facts, we estimated that the error bars on the temperature are of the order of ±40 000 K (see Fig. 5).

4. Comparison with the MHD model

The observed loop is modelled using steady 2D MHD equilibrium solutions with compressible unidirectional flow (Petrie et al. 2002, 2003). The details of the modelling technique, including a self-consistent heating model, are described fully in

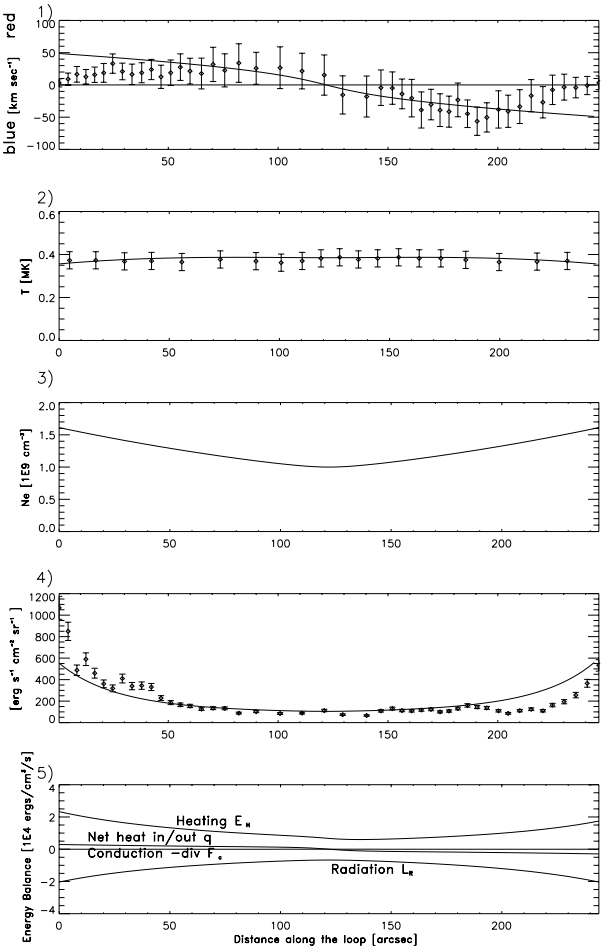

Fig. 6. A summary of the measurements we carried out along the loop, fitted with the MHD model. The data are represented as diamonds with their error bars and the MHD computations are the full lines. Here, the modelled flow is projected along the LOS so that we can compare with the data. In panel 2, the temperatures were constrained using the Emission Measure curves (see Fig. 5). Panel 3 shows the computed electron density along the loop. The computed temperatures and electron densities are used to compute the intensity in the O V spectral line, which is compared with the observed one in panel 4. In panel 5, where we do not have any data measurements, we present the terms of the energy balance along the loop. The heating $E_{\rm H}$ is the resulting energy from the balance of the other terms. Note that the conductive losses are very small in the scale of panel 5.

Petrie et al. (2003). The use of a steady model to describe the observed loop is justified since the time scale involved in the observed loop (roughly 1 h as seen in Fig. 1) is significantly larger than the time for a disturbance to travel along the loop with an Alfvén speed of 1000 km s^{-1} (less than 4 min as the loop length is 225 Mm, see Sect. 2).

Moreover, for a radiative loss rate at 380 000 K of $\Lambda\,(T) \approx 10^{-10.4} T^{-2}$ (Rosner et al. 1978) and an electron density of 10^9 cm^{-3}, the cooling time is $\tau = \frac{3\,k_{\rm B}\,T}{n_{\rm e}\,\Lambda(T)} \approx 10$ min. This is considerably smaller than the loop lifetime. Therefore we consider that the loop is in thermal equilibrium.

Given the loop dimensions, the model computes the flow, the mass density, temperature and heating along the loop, for a calculated shape of the magnetic field. The computed loop geometry is orientated in space by tuning two angles, so that the loop projection on the plane of the sky fits the observed loop shape (see Petrie et al. 2003, for further details). One more constraint to this operation is that the computed line of sight velocity should fit the observed Doppler shifts (see Fig. 6, panel 1).

From the computed electron densities and temperatures, we calculated an O V intensity flux along the loop, which was compared to the observed flux (see Fig. 6, panels 2–4). This forward process supposed that:

- the loop differential emission measure along the LOS is described by a Dirac function centered at the computed temperature;
- the loop width is constant and equal to 4 Mm along the loop;
- the filling factor is taken to be equal to 1 but our model is qualitatively unchanged for filling factors down to the order of 0.5.

From Fig. 6 we see that the model succesfully represents the smooth drop of the intensity along the loop. Recall that hydrodynamic siphon flow calculations do not produce the large intensity scale heights along O V loops observed at the limb by CDS except if an ad hoc constant temperature is imposed along the modeled loop (Peres 1997).

In panel 4, we present graphs of the functions involved in the energy equation. The radiative term ($L_{\rm R}$), being negative to represent an energy loss, dominates the energy balance, and conduction (div $F_{\rm c}$) is negligible because the model is nearly isothermal. The net heat in/out (q) is computed from the first law of thermodynamics, (see Petrie et al. 2003, Eq. (3)). Due to its dependence on the flow it is anti-symmetric. From the summation of the above mentioned energy terms we compute the unknown heating distribution along the loop ($E_{\rm H}$) which safeguards energy conservation. From Fig. 6 we see that $E_{\rm H}$ has a minimum near the loop top, local maxima at the footpoints and is stronger at the upflow footpoint. Moreover, we deduce the heating function without any assumption about which mechanism is producing this heating, simply from the energy conservation.

5. Discussion

Coronal loops are almost always modelled using hydrostatic or hydrodynamic solutions, i.e. solutions that do not explicitly include the magnetic field. However, in real plasma systems the magnetic field inevitably causes the plasma to depart from one-dimensional equilibrium, particularly in such a magnetized, sparse medium as the solar corona. Even near-isothermal images of near-static active regions show disagreement with hydrostatic equilibrium in their characteristic density scale height and complex structure (Aschwanden et al. 2001, Fig. 8). The graph of density against arclength of a field line in a hydrostatic plasma is likely to differ from that of a field line of identical size and shape in a non-force-free magnetohydrostatic plasma of the same characteristic temperature. This is reflected in the fact that the isobars and isotherms of non-force-free MHD models are generally very different from the isobars and isotherms of hydrostatic equilibrium, which are parallel to the photosphere.

The physical parameters along a steady MHD loop can differ from hydrostatic equilibrium because the cross-field compressive forces are generally not distributed along the loop in the same manner as the usual field-aligned hydrostatic forces (Petrie et al. 2003). The justification for excluding this direct participation of the magnetic field in traditional hydrostatic and hydrodynamic models is that the Lorentz force is perpendicular to the magnetic field and therefore does not influence the statics/dynamics along the loop. However in 2D and 3D magnetic structures the Lorentz force communicates across the loop with the pressure gradient, gravitational and inertial forces, giving rise to the various scale heights found in near-isothermal images.

In the study by Aschwanden et al. (1999), EUV loops observed by EIT on the disc are fitted with hydrostatic models. With one small exception, only parts of loops were amenable to measurement and modelling. Hydrostatic models were successfully fitted to these loop parts. Then, Aschwanden et al. (2001) selected entire TRACE loops on the limb and concluded from hydrostatic modelling that the observed scale heights were super-hydrostatic.

Furthermore, the cases of flat temperature and density profiles measured along loops, observed by imagers as well as by CDS, cannot be reproduced by steady hydrodynamic flow models (Patsourakos et al. 2004; Landi & Landini 2004). Such tests should be repeated for loops where the measured temperature decreases toward the footpoints (e.g. Del Zanna & Mason 2003).

However, MHD physics produces steady loop solutions that can easily fit the temperature and density profiles deduced by $\simeq 10^6$ K loops (Petrie et al. 2003). Therefore, it appears that MHD steady flows may be useful for the study and understanding of coronal loops, despite their limitations which we discuss in the following.

One limitation of our modelling technique, compared with other techniques, is that the loop cross section increases from the footpoint upward, contrary to the observational evidence. This is a consequence of the self-similarity technique invoked in order to generate the analytical solutions (Petrie et al. 2002): any two field lines can only differ by a vertical translation. It is not obvious how to re-derive the solutions maintaining some freedom in the loop width function. Various 1D techniques allow free width functions by ignoring the cross-field physics. In two dimensions we do not have this luxury. Instead, we can interpret our results taking this limitation into account.

Because the model loop legs are nearly vertical, our modelled loop is much narrower at the footpoints than at the apex. Thus, the model overestimates the plasma velocity near the footpoints, (cf., top panel in Fig. 6). A model with a nearly constant cross-section and the same mass flux would better reproduce the decrease in velocity magnitude seen in the observations.

As a consequence of the smaller width of the loop at the footpoints, the model over-estimates the magnetic field strength, which in turn affects the plasma parameters, e.g. in the present model the gas pressure and the temperature drop. While the model is reasonable over most of the loop length, it is weaker in the sections within $40''$ of each footpoint. This is a small price to pay for a reasonable full MHD description over most of the loop length.

A trace of the enhanced heating at the upflow leg can be seen in the enhanced line width that the O V line presents at the loop legs. However, the instrument broadening of the line profiles is very large for CDS, so we can use this as a hint. Another indication could be the fact that the north leg, is near a bright region, visible in all images (see Fig. 3) which had a strong brightening during the flare observed by Yohkoh.

TRACE observations, due to the higher spatial resolution, revealed the multistrand structure of loops, which has not been taken into account in the present study. Various attempts have been made to model loops as bundles of many independent strands, each of them in hydrostatic equilibrium, by simply superposing solutions (Aschwanden et al. 2000; Reale & Peres 2000). A major problem with this multistrand approach, however, is that, while the hydrostatic equation is linear in its physical parameters, the energy equation is highly nonlinear (as are the hydrodynamical and MHD equations) so that two independent solutions do not add together to form a new solution, in general. However, Sakai & Furusawa (2002) did take into account this nonlinearity in a multi-thread model with flow, using a full 3D MHD code, but they do not include the loop curvature in their model.

6. Conclusions

We have compared detailed observations of flows and intensities in a cool solar loop with a 2D-MHD model. We presented evidence that the plasma material is feeding the selected loop from the north footpoint, as one can see from the first three intensity images in Fig. 1. This, in combination with the Doppler shifts (Fig. 2), strongly indicates a unidirectional flow along the loop. The temperature has been also estimated, at first order, to be around 380 000 K and seems to remain nearly constant along the loop length.

The three data sets (intensity, velocity and temperature), along with the loop geometry, represent a sufficient constraint for the free parameters of the MHD model. From the resulting fitting process, we computed the energy terms that participate in the energy balance and we deduced the shape of the heating function along the loop. The heating function is stronger at the footpoints. Moreover, the heating function presents an asymmetry, being stronger at the upflowing leg. This may be a serious constraint for modelling the mechanism that produces this heating function; nevertheless, this is beyond the scope of this work. The measure of the non-thermal broadening of the spectral line along the loop used to deduce the flows (O V in our case) can give information on the shape of the heating function (see also Spadaro et al. 2000). In our case however, due to the degradation of the CDS instrument after the loss of SOHO, this was not possible.

The shape of the heating function is likely to generalise across all models constructed in this way. A model with symmetric plasma parameter profiles and unidirectional flow will always have symmetric radiative loss and heat conduction profiles, as well as an anti-symmetric net heat in/out function (first law of thermodynamics). For near-isothermal loops, heat con-

duction does not contribute much to the energy equation and the radiative losses are concentrated at the footpoints in any model with gravitational stratification. The heating balance will therefore balance a combination of a symmetric radiative loss function and an antisymmetric net heat in/out function. Such a combination can only give an asymmetric heating function, concentrated at the footpoints and biased towards the upflow footpoint. This bias is determined by the radiative loss function and the net heat in/out function.

Using a 3D MHD code, Gudiksen & Nordlund (2002) give a 3D numerical model where photospheric motion followed by field-line relaxation results in footpoint heating by magnetic dissipation that causes heated plasma to fill the loop from one footpoint to the other. It is reassuring that their approach also predicts that biased footpoint heating is consistent with unidirectional plasma flow.

In our previous work (Petrie et al. 2003), we deduced the same characteristics of the heating function for three other loops. However, we had studied loops that were in the temperature range of $(1.-1.5 \times 10^6)$ K, whereas in this case, the loop is much cooler. More loops, with clear unidirectional flows, should be studied in order to fully explore this new mathematical tool.

Acknowledgements. C.G. and G.P. acknowledge funding by the EU Research Training Network PLATON, contract number HPRN-CT-2000-00153. C.G. also acknowledges support from a Greek-French bilateral agreement (Program Platon), the Research Comittee of the Academy of Athens and the Costopoulos Foundation. We also thank T. Fredvik for reading a previous version of the manuscript, as well as the anonymous referee for the valuable comments which contributed to a significant improvement of our paper. CHIANTI is a collaborative project involving the NRL (USA), RAL (UK) and the Universities of Florence (Italy) and Cambridge (UK), while SOHO is a joint project of ESA and NASA.

References

Aschwanden, M. J. 2002, ApJ, 580, 79
Aschwanden, M. J., Newmark, J. S., Delaboudinière, J. P., et al. 1999, ApJ, 515, 842
Aschwanden, M. J., Nightingale, R. W., & Alexander, D. 2000, ApJ, 541, 1059
Aschwanden, M. J., Schrijver, C. J., & Alexander, D. 2001, ApJ, 550, 1036
Bradshaw, S. J., & Mason, H. E. 2003a, A&A, 401, 699
Bradshaw, S. J., & Mason, H. E. 2003b, A&A, 407, 1127
Bray, R. J., Cram, L. E., Durrant, C. J., & Loughhead, R. E. 1991, Plasma Loops in the Solar Corona (Cambridge University Press)
Brekke, P. 1999, Sol. Phys., 190, 379
Brekke, P., Kjeldseth-Moe, O., & Harrison, R. A. 1997, Sol. Phys., 175, 511
Del Zanna, G. 1999, Ph.D. Thesis, Univ. of Central Lancashire, UK
Del Zanna, G., Bromage, B. J. I., Landi, E., & Landini, M. 2001, A&A, 379, 708
Del Zanna, G., & Mason, H. E. 2003, A&A, 406, 1089
Dere, K. P. 1982, Sol. Phys., 75, 189
Dere, K. P., Landi, E., Mason, H. E., Monsignori Fossi, B. C., & Young, P. R. 1997, A&AS, 125, 149
Fludra, A., Brekke, P., Harrison, R. A., et al. 1997, Sol. Phys., 175, 487
Fludra, A., & Schmelz, J. T. 1999, A&A, 348, 286
Foukal, P. V. 1975, Sol. Phys., 43, 327
Foukal, P. V. 1976, ApJ, 210, 575
Fredvik, T., Kjeldseth-Moe, O., Haugan, S. V. H., et al. 2002, AdSpR, 30, 635
Gudiksen, B. V., & Nordlund, Å. 2002, ApJ, 572, L113
Habbal, S. R., Ronan, R., & Withbroe, G. L. 1985, Sol. Phys., 98, 323
Judge, P. G., & McIntosh, S. W. 2000, Sol. Phys., 190, 331
Kjeldseth-Moe, O., & Brekke, P. 1998, Sol. Phys., 182, 73
Landi E., & Landini, M. 2004, ApJ, 608, 1133
Lenz, D. D., DeLuca, E. E., Golub, L., Rosner, R., & Bookbinder, J. A. 1999, ApJ, 517, 155
Martens, P. C. H., Cirtain, J. W., & Schmelz, J. T. 2002, ApJ, 577, 115
Mazzotta, P., Mazzitelli, G., Colafrancesco, S., & Vittorio, N. 1998 A&AS, 133, 403
Patsourakos, S., Klimchuk, J. A., & MacNeice, P. J. 2004, ApJ, 603, 322
Peres, G. 1997, in Proceedings of the Fifth SOHO Workshop, The Corona & Solar Wind near Minimum Activity, ed. A. Wilson (Noordwijk: ESA), ESA SP-404, 55
Peter, H., & Judge, P. G. 1999, ApJ, 522, 1148
Petrie, G. J. D., Vlahakis, N., & Tsinganos, K. 2002, A&A, 382, 1092
Petrie, G. J. D., Gontikakis, C., Dara, H. C., Tsinganos, K., & Aschwanden, M. J. 2003, A&A, 409, 1065
Sakai, J. I., & Furusawa, K. 2002, ApJ, 564, 1048
Schmelz, J. T., Scopes, R. T., Cirtain, J. W., Winter, H. D., & Allen, J. D. 2001, ApJ, 556, 896
Schmelz, J. T., Saba, J. L. R., Ghost, D., & Strong, K., T. 1996, ApJ, 473, 519
Sheeley, N. R. 1980, Sol. Phys., 66, 79
Shull, J., & Van Steenberg, M. 1982, 48, 95
Spadaro, D., Antiochos, S., K., & Mariska, J. T. 1991, ApJ, 382, 338
Spadaro, D., Lanzafame, A. C., Consoli, L., et al. 2000, A&A, 359, 716
Reale, F., & Peres, G. 2000, ApJ, 582, L45
Rosner, R., Tucker, W. H., & Vaiana, G. S. 1978, ApJ, 220, 643
Thompson, W. T., CDS Software note No. 53, `http://solg2.bnsc.rl.ac.uk/software/notes.shtml`
Winebarger, A. R., Warren, H. P., & Mariska, J. T. 2003 ApJ, 587, 439